Tailoring Graphene Oxide-Based Aerogels for Efficient Solar Steam Generation under One Sun

*Xiaozhen Hu, Weichao Xu, Lin Zhou, Yingling Tan, Yang Wang, Shining Zhu, and Jia Zhu**

Solar steam generation is emerging as one of the most promising solar energy technologies, for its potential applications in water desalination[1,2] and purification,[3] distillation and liquid–liquid phase separation,[4,5] and sterilization.[6] As the efficiency of solar steam generation depends strongly on the absorbers, which absorb light and transfer the energy to water nearby for steam generation, various absorbers, including suspended metallic nanoparticles,[4–6] carbon materials,[7–10] and plasmonic absorbers,[11,1,3,12–16] have been developed for vapor generations. However, so far high solar steam efficiency (>80%) has only been achieved under concentrated sunlight, which can limit the scalability of technologies. Through recent progress, it becomes clear that ideal absorbers should possess several properties: broadband and efficient solar absorption, reduced thermal conductivity for localized water heating, hydrophilicity for efficient water supply, and porous networks for vapor channels.

Aerogels are emerging as one novel kind of porous solids[17] with many fascinating properties such as low mass density, high porosity, large surface area, and low thermal conductivity. Since the first study by Kistler in 1930s,[18] various kinds of aerogels such as silica aerogels,[19–21] metal aerogels,[22] polymer aerogels,[23,24] and carbon aerogels[17,25–32] have been fabricated,[33] with promising applications in energy storage,[17,32–35] catalysis,[17] hydrogen storage,[36] and CO_2 adsorption.[37] In this work, for the first time we demonstrate that graphene oxide (GO)-based aerogels with carefully tailored absorption, thermal, and hydrophilic properties can enable efficient (≈83%) solar steam generation under one-sun illumination.

GO, as one of the most important derivatives of graphene,[35,38] has good dispersibility, providing opportunities to precisely tailor the nano- and microstructures of the GO assemblies through solution processes.[39–41] There are several unique features regarding GO aerogels beneficial for efficient solar steam generation. First, GO aerogels, with intentionally introduced multiwalled carbon nanotubes (MWCNTs), can enable broadband and efficient solar absorption (≈92%). Second, the intrinsic low thermal conductivity (<0.05 W m^{-1} K^{-1})[24,42,43] of aerogels enables desirable heat localization for steam generation. Third, by addition of biocompatible sodium alginate (SA), GO aerogels demonstrate good hydrophilicity with water contact angle up to 74°. The inherent porous networks offer aerogels with water supply and vapor escape channels, as well as low density (1.2–17.6 mg cm^{-3}), which can make aerogels float naturally on the surface of water. All of these properties are carefully examined below. With these intrinsic features and tailored characteristics, our GO aerogels serve as idea absorbers for efficient solar steam generation.

Scheme 1 shows the fabrication processes of a GO-based aerogel. GO, SA, and MWCNTs were dispersed in water and mixed adequately by alternative ultrasonication and stirring. The mixture was then freezed in the polytetrafluoroethylene (PTFE) mode by liquid nitrogen. Followed by a conventional freezing-drying procedure, GO-based aerogels were obtained (more details in the Experimental Section). During the freezing process of GO-SA-CNT dispersion, the ice crystals grow along the axis of mode because of temperature gradient generated by the liquid nitrogen and eventually produce one piece of frozen materials consisting of ice crystals surrounded by the walls formed by the dispersed GO platelets, SA molecules, and CNTs. Freezing-drying removes the ice crystals by sublimating ice into vapor subsequently, leaving the porous framework connected by the GO-SA-CNT walls. To improve the absorption, GO can be partially reduced to Rrduced graphene oxide (RGO) by convenient thermal treatment. The resulting RGO-SA-CNT aerogel has a shape of a black cylinder, with 25 mm in diameter and 5 mm in height (**Figure 1**a,b). Because of high porosity, aerogels are famous for their ultralight property, which can be placed on a fragile metasequoia leaf without changing its shape (Scheme 1).

For optimizing the water transporting distance during the solar steam generation, the aerogel can be conveniently pressed from 5 mm (Figure 1b) to 1.5 mm thick (Figure 1c, which is optimized for steam generation test, Figure S1, Supporting Information). Scanning electron microscopy (SEM) image shows RGO sheets form the porous framework and the pore size is mainly in the range of 30–50 μm before being pressed (Figure 1d). After being pressed, the pore size was reduced to 10–30 μm (Figure 1e). Surface area measured by N_2 adsorption is found to be ≈125 m^2 g^{-1} (Figure S2, Supporting Information). The porous microstructures and defects on RGO sheets provide aerogels excellent thermal insulating properties,[24,42–44] quick vapor escape as well as channels for liquid supply. The density of pressed RGO-SA-CNT aerogels is around 8 mg cm^{-3}, which allows the aerogels free-floating on the top surface of water.

Figure 1f shows the zoom-in SEM picture of aerogels with RGO sheets assembled around the pores. High-resolution SEM

Dr. X. Z. Hu, W. C. Xu, Dr. L. Zhou, Y. L. Tan, Y. Wang, Prof. S. N. Zhu, Prof. J. Zhu
National Laboratory of Solid State Microstructures
College of Engineering and Applied Sciences
and Collaborative Innovation Center
of Advanced Microstructures
Nanjing University
16 Jinyin Street, Nanjing 210093, P. R. China
E-mail: jiazhu@nju.edu.cn

DOI: 10.1002/adma.201604031

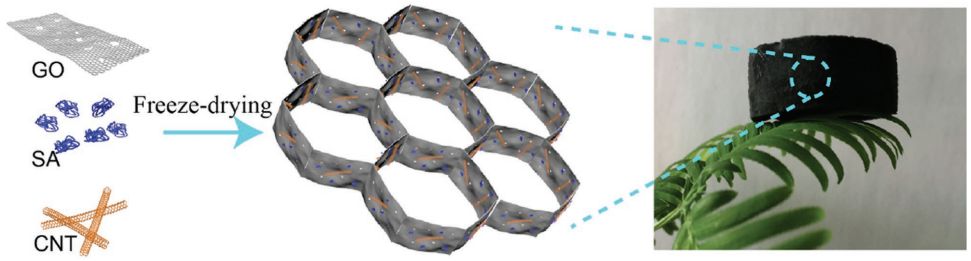

Scheme 1. The fabrication process of GO-based aerogels. GO, SA, and CNT were first mixed in water and followed by a freeze-drying process, GO-SA-CNT aerogels were obtained.

image shows that RGO sheets are relatively flat and smooth in the RGO aerogels (Figure 1g). After addition of CNT and SA, the sheets become much more wrinklable (Figure 1h). SA and CNT are distributed evenly on the GO walls with no obvious aggregation observed, suggesting the aerogel possesses a high degree of homogeneity.

The surface chemical compositions and functional groups of the GO, RGO, RGO-SA, and RGO-SA-CNT aerogels were identified by X-ray photoelectron spectroscopy (XPS), as shown in **Figure 2**a and Figure S3 (Supporting Information). As expected, for GO and RGO, only C 1s and O 1s signals were detected in the XPS survey spectra. After addition of SA, a new peak located at 1071 eV is observed in both the RGO-SA and RGO-SA-CNT, corresponding to Na 1s. Another peak appearing at 402 eV for RGO-SA-CNT can be attributed to N 1s induced by hexadecyl trimethyl ammonium bromide (CTAB), which is added to the suspension of MWCNTs to improve the dispersibility. GO aerogels show a C/O ratio of 1.94 and this value increases to 4.38 for RGO after the thermal treatment, and the total O content reduced from 34 to 18.6 at%, indicating the partial reduction of GO. The deconvoluted C 1 s spectra of GO aerogels show three peaks at 284, 286.1, and 287.7 eV (Figure S3, Supporting Information), corresponding to C—C/C=C, C—O, and C=O, respectively.[45] After reduction, the intensity of epoxy groups decreases significantly, while the peak intensity corresponding to carboxyl carbon decreases slightly. Different from graphene,[44] the residual carboxyl and epoxy groups can introduce defects on the perfect sp^2 framework, leading to low thermal conductivity,[42,43] as explained below.

Absorption of aerogels was measured with an ultraviolet-visible-near-infrared spectrophotometer equipped with an integrating sphere. As shown in Figure 2b, the averaged absorption (weighted by AM1.5G solar spectrum) across 200–2500 nm is 82% for neat RGO aerogels. To increase the absorption of solar energy, MWCNTs as excellent absorbers[46] were added to aerogels. The absorption increases to ≈92% for the RGO-SA-CNT aerogels, which lays foundations for efficient solar steam generation.

As hydrophilicity is important to enable efficient water supply for solar steam generation, water wetting performance of aerogels was quantitatively measured by water contact angles. RGO aerogels show hydrophobic property with water contact angle of 115°. With addition of SA, a good water adsorbent, the water contact angle of RGO-SA reduces to 74° (Figure S4, Supporting Information), showing excellent hydrophilic property. Therefore, water can soak through the interconnected pores of aerogels rapidly, which ensuring efficient water supply during steam generation. Apart from providing transportation channels for water, the porous structure is favorable to reduce the thermal conductivity. Graphene foams synthesized by chemical vapor

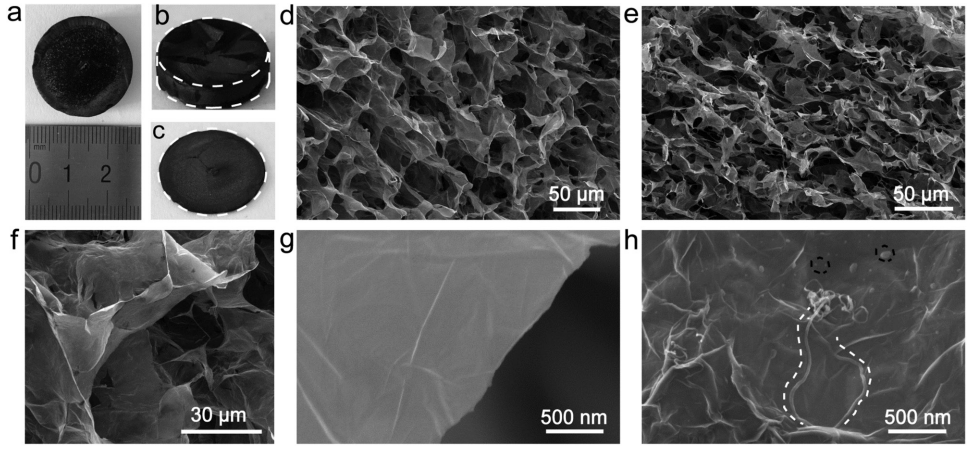

Figure 1. Morphology of GO-based aerogels. a) Top view of the as-prepared RGO-SA-CNT aerogel, showing the diameter of aerogels is 25 mm. Side view of the RGO-SA-CNT aerogel b) before and c) after being pressed. SEM images of RGO-SA-CNT aerogels d,f) before and e) after being pressed. Along with the aerogels height changes from 5 to 1.5 mm, the pore diameter decreases. High-resolution SEM images of g) RGO aerogels and h) RGO-SA-CNT aerogels. The white and black dashed lines in (h) show the appearance of CNT and SA, respectively.

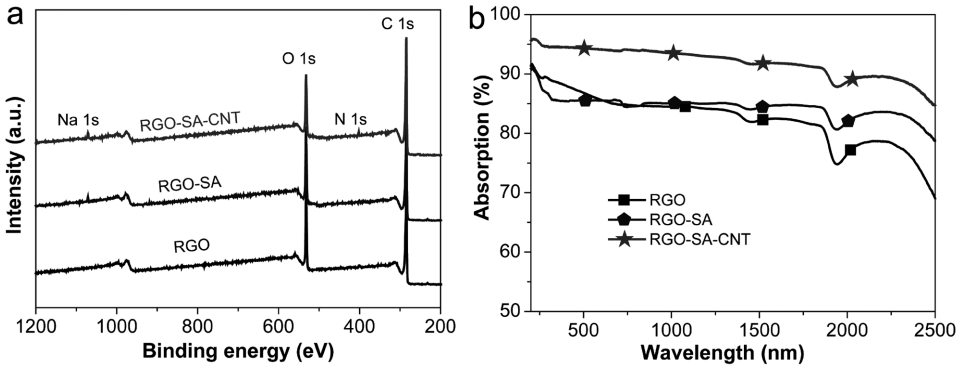

Figure 2. a) XPS and b) absorption spectra of RGO, RGO-SA, and RGO-SA-CNT aerogels.

deposition on Ni foam templates demonstrate thermal conductivity of 0.26–350 W m^{-1} K^{-1} at RT.[9,44] GO aerogels show much more lower thermal conductivity (0.0047–0.035 W m^{-1} K^{-1} at RT), which has mainly ascribed to the defects on the graphene skeleton.[42,43] Such a low thermal conductivity is beneficial for localized water heating, critical for efficient solar steam generation (Figure S5, Supporting Information).

The efficient absorption across the full solar spectrum, good wettability, together with the porous structure which enables efficient water supply and vapor channel and very low thermal conductivity make RGO-SA-CNT aerogels ideal absorbers for solar steam generation. To quantitatively characterize the performance of RGO-SA-CNT aerogels, the energy transfer efficiency was carefully examined by measuring the water evaporation rate in a thermally insulated chamber. The aerogel was free-floating on the water due to the low density (1.2–17.6 mg cm^{-3}), with water diffused all around the sample ascribed to the excellent hydrophilic property and interconnected water channels. Once the light is on, the mass change of water due to the steam generation was carefully tracked by a balance. The typical curves of time-dependent mass change were provided in **Figure 3**a. Evaporation rates were calculated from the slope of the curves. For pure water, the water evaporation rate is 0.500 kg m^{-2} h^{-1}, after addition of RGO aerogels, the rate increases to 1.056 kg m^{-2} h^{-1}, which is two times that of pure water. The evaporation rate further increases to 1.395 kg m^{-2} h^{-1} after introducing the water adsorbent SA into RGO aerogels. The highest water evaporation rate of 1.622 kg m^{-2} h^{-1} was achieved for RGO-SA-CNT aerogels (Figure 3b), indicating the introduction of SA and CNT dramatically improves the evaporation rate.

The energy conversion efficiency is defined as $\eta = mh_{lv}/P_{in}$, where m is the mass flux of steam, h_{lv} denotes the liquid-vapor phase change enthalpy, and P_{in} is the power density of solar illumination. The efficiency of RGO-SA-CNT aerogels can achieve 83% at power density of 1 kW m^{-2}, higher than that of neat RGO aerogels (56%) and most of previous reports (typically 60–70%) under one-sun illumination.[7,10,12,13] Therefore it is confirmed that RGO-SA-CNT aerogels with 92% absorption, low thermal conductivity (<0.05 W m^{-1} K^{-1}), good hydrophilicity (≈74°), and porous networks can serve as ideal absorbers for efficient solar steam generation.

To further investigate heat localization caused by aerogels under one-sun intensity, infrared camera was used to capture the temperature (T) variations across the beakers. **Figure 4**a compares the T of RGO-SA-CNT surface and water at the bottom over time irradiation. After 1 h light illumination, the T of the free-floating aerogel showed a sharper T increase than that of water in the bottom. The T on the aerogel surface increases from 25 to 36 °C within 1000 s illumination, and then further to 40 °C within 1 h. In contrast, the T of bottom water maintained around 28 °C (from 25 °C) after 1000 s irradiation and 31 °C after 1 h. Insets in Figure 4a are infrared photographs of the beaker with irradiation time of 0 s, 1000 s, and 1 h, respectively. In addition, we also carefully measured

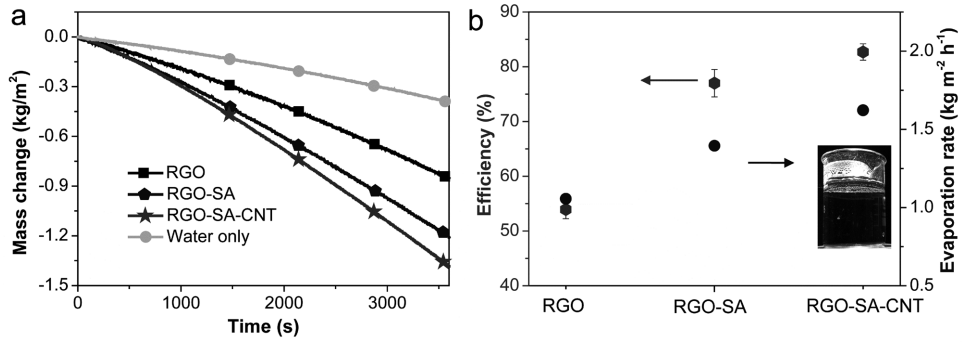

Figure 3. GO-based aerogels for steam generation. a) Mass change of water with different absorbers over time at an optical density of 1 kW m^{-2}. b) Solar steam efficiency (hexagon, left-hand side axis) and evaporation rate (circle, right-hand side axis) with different aerogels absorbers.

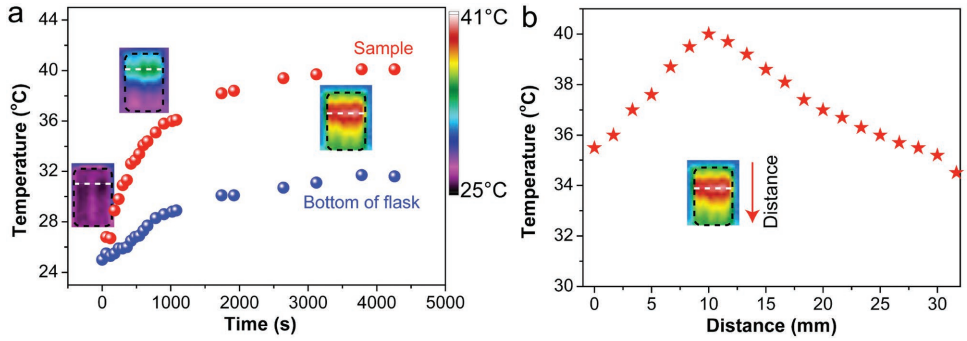

Figure 4. Heat localization behavior of GO-based aerogels. a) The temperature of RGO-SA-CNT aerogels and bottom water under the solar light irradiation as a function of time. The inset shows infrared photos of the beaker after 0 s, 1000 s, and 1 h illumination at 1 kW m^{-2}. Black dashed lines are the contour of beaker and the white lines are the position of free-floating sample. b) Temperature profiles along the beaker axis after 1 h illumination at 1 kW m^{-2}. Inset is the corresponding infrared photos of RGO-SA-CNT aerogels.

the T of water at bottom, right below the aerogel, and inside the aerogel in the Dewar flask (Figure S6, Supporting Information). Both results confirmed that aerogel can use the absorbed energy to heat the water at the top surface without heating the bulk water, which is beneficial for efficient solar steam generation. Figure 4b shows the sharp T gradient along the beaker axis of RGO-SA-CNT aerogels after 1 h irradiation, indicating the interfacial heating attribute of our aerogels.

In conclusion, we demonstrated that a free-floating GO-based aerogels with carefully tailored properties can enable highly efficient solar steam generation. The RGO-SA-CNT aerogels, with porous structures built up with RGO sheets together with CNT and SA, possess excellent absorption of solar spectrum (≈92% across 200–2500 nm), good hydrophilicity and porous networks for efficient water supply and vapor channels, and thermal insulating property for heat localization, and therefore can enable about 83% energy transfer efficiency under one-sun illumination (1 kW m^{-2}). With scalable materials and processes, carefully tailored properties, high energy transfer efficiency under normal sunlight, it is expected that this type of aerogel-based solar steam generation promises wide range of applications such as desalination, water purification, and sterilization.

Experimental Section

Materials Preparation: GO was synthesized from natural graphite powder (40 µm in size, Qingdao Henglide Graphite Co., Ltd.) using the modified Hummers method. SA was purchased from Sigma-Aldrich and dissolved in water with a concentration of 10 mg mL^{-1}. Multiwalled carbon nanotubes (MWCNTs) were provided by Prof. Fei Wei in Tsinghua University and were dispersed in water (1 mg mL^{-1}) with the aid of CTAB surfactant and sonication. GO (18 mg) was dispersed in deionized water (15 mL), giving the GO precursor; GO (18 mg) and SA (3.6 mg) were mixed by stirring for 1 h in water (15 mL), providing the GO-SA precursor; GO (18 mg), SA (6 mg), and MWCNTs (6 mg) were mixed by alternative sonication and stirring in water (15 mL), leading to the GO-SA-CNT precursor. The ratio of MWCNTs was optimized by the absorption and mechanical stability (Figure S7, Supporting Information). These three kinds of precursors were transferred into the PTFE mode with 25 mm in diameter and 5 mm in depth, respectively. After freezed by the liquid nitrogen, these frozen dispersions were freeze dried for 48 h, followed by 150 °C treatment in vacuum for 12 h, RGO, RGO-SA, and RGO-SA-CNT aerogels with 25 mm in diameter and 5 mm in height were obtained.

Materials Characterizations: The morphologies and structures of the as-prepared aerogel were characterized by scanning electron microscopy (Dual-beam FIB 235, FEI Strata). XPS spectra were obtained on THERMO FISHERSCIENTIFIC K-Alpha. The optical transmittance and reflectance spectra of the aerogel were measured in the range of 200–2500 nm with a Shimadzu UV3600 spectrophotometer attached to an integrating sphere (ISR-3100). The absorption efficiency was then calculated by $A = 1 - R - T$, R and T are the reflection and transmission efficiency, respectively. The specific surface area of the aerogel was measured by Thermo Fisher Scientific Surfer Gas Adsorption Porosimeter with N_2 as absorbate. FLUKE Ti 100 infrared camera was used to take infrared photographs. Thermal diffusivity was measured by Netzsch LFA 467 Nanoflash. Water contact angles were measured using a contact angle meter (DSA 100, KRUSS incorporation in German). The contact angle was measured by a contact angle goniometer using an optical subsystem to capture the profile of a water drop on the aerogel sample. The angle formed between the liquid–solid interface and the liquid–vapor interface is the contact angle. The mechanical tests were performed on a Microcomputer Control Electronic Universal Testing Machine made by REGER in China (RGWT-4000-5) (Figure S8, Supporting Information).

Experimental Set-Up for Steam Generation: The steam generation experiments were performed under a homemade optical system, with a solar simulator (Newport 94043A) and a double-lens focusing components (Beijing optical century instrument). The experiments were typically conducted at an ambient T of 25 °C and humidity of ≈45%. The designed test chamber was a Dewar flask (28 mm inner diameter, 38 mm outer diameter, and 96 mm height; Shanghai Glass Instrument Co.). In the experiment, the water was contained by a chamber and the aerogel floated on the surface of the water. The mass change was measured by a high accuracy balance (FA 2004, 0.1 mg in accuracy) and then real-time communicated to a desktop computer for the evaluation of the evaporation rate and solar-thermal conversion efficiency.

Supporting Information

Supporting Information is available from the Wiley Online Library or from the author.

Acknowledgements

The authors thank Prof. F. Wei of Tsinghua University for providing the multiwalled carbon nanotubes, Prof. J. Xu of Nanjing University for the

absorption test, Prof. X. Z. Wang and Prof. Z. Hu of Nanjing University for helping to test surface area.

This work was jointly supported by the State Key Program for Basic Research of China (Grant No. 2015CB659300), National Natural Science Foundation of China (NSFC Nos. 11321063 and 11574143), Natural Science Foundation of Jiangsu Province (Grant No. BK20150056), the Priority Academic Program Development of Jiangsu Higher Education Institutions (PAPD), and the Fundamental Research Funds for the Central Universities.

Received: July 29, 2016
Revised: October 14, 2016
Published online: November 25, 2016

[1] L. Zhou, Y. L. Tan, J. Y. Wang, W. C. Xu, Y. Yuan, W. S. Cai, S. N. Zhu, J. Zhu, *Nat. Photonics* **2016**, *10*, 393.
[2] Y. C. Wang, L. B. Zhang, P. Wang, *ACS Sustainable Chem. Eng.* **2016**, *4*, 1223.
[3] Y. Liu, J. W. Lou, M. T. Ni, C. Y. Song, J. B. Wu, N. P. Dasgupta, P. Tao, W. Shang, T. Deng, *ACS Appl. Mater. Interfaces* **2016**, *8*, 772.
[4] O. Neumann, A. D. Neumann, E. Silva, C. Ayala-Orozco, S. Tian, P. Nordlander, N. J. Halas, *Nano Lett.* **2015**, *15*, 7880.
[5] O. Neumann, A. S. Urban, J. Day, S. Lal, P. Nordlander, N. J. Halas, *ACS Nano* **2013**, *7*, 42.
[6] O. Neumann, C. Feronti, A. D. Neumann, A. Dong, K. Schell, B. Lu, E. Kim, M. Quinn, S. Thompson, N. Grady, P. Nordlander, M. Oden, N. J. Halas, *Proc. Natl. Acad. Sci. USA* **2013**, *110*, 11677.
[7] H. Ghasemi, G. Ni, A. M. Marconnet, J. Loomis, S. Yerci, N. Miljkovic, G. Chen, *Nat. Commun.* **2014**, *5*, 4449.
[8] G. Ni, N. Miljkovi, H. Ghasemi, X. P. Huang, S. V. Boriskina, C. T. Lin, J. J. Wang, Y. F. Xu, M. M. Rahman, T. J. Zhang, G. Chen, *Nano Energy* **2015**, *17*, 290.
[9] Y. Ito, Y. Tanabe, J. H. Han, T. Fujita, K. Tanigaki, M. W. Chen, *Adv. Mater.* **2015**, *27*, 4302.
[10] L. B. Zhang, B. Tang, J. B. Wu, R. Y. Li, P. Wang, *Adv. Mater.* **2015**, *27*, 4889.
[11] Y. M. Liu, S. T. Yu, R. Feng, A. Bernard, Y. Liu, Y. Zhang, H. Z. Duan, W. Shang, P. Tao, C. Y. Song, T. Deng, *Adv. Mater.* **2015**, *27*, 2768.
[12] L. Zhou, Y. L. Tan, D. X. Ji, B. Zhu, P. Zhang, J. Xu, Q. Q. Gan, Z. F. Yu, J. Zhu, *Sci. Adv.* **2016**, *2*, e1501227.
[13] K. Bae, G. Kang, S. K. Cho, W. Park, K. Kim, W. J. Padilla, *Nat. Commun.* **2015**, *6*, 10103.
[14] S. T. Yu, Y. Zhang, H. Z. Duan, Y. M. Liu, X. J. Quan, P. Tao, W. Shang, J. B. Wu, C. Y. Song, T. Deng, *Sci. Rep.* **2015**, *5*, 13600.
[15] L. M. Tian, J. Y. Luan, K. K. Liu, Q. S. Jiang, S. Tadepalli, M. K. Gupta, R. R. Naik, S. Singamaneni, *Nano Lett.* **2016**, *16*, 609.
[16] Z. H. Wang, Y. M. Liu, P. Tao, Q. C. Shen, N. Yi, F. Y. Zhang, Q. L. Liu, C. Y. Song, D. Zhang, W. Shang, T. Deng, *Small* **2014**, *10*, 3234.
[17] J. Biener, M. Stadermann, M. Suss, M. A. Worsley, M. M. Biener, K. A. Rose, T. F. Baumann, *Energy Environ. Sci.* **2011**, *4*, 656.
[18] S. S. Kistler, *Nature* **1931**, *127*, 741.
[19] T. M. Tillotson, L. W. Hrubesh, *J. Non-Cryst. Solids* **1992**, *145*, 44.
[20] C. A. Morris, M. L. Anderson, R. M. Stroud, C. I. Merzbacher, D. R. Rolison, *Science* **1999**, *284*, 622.
[21] J. V. Ryan, A. D. Berry, M. L. Anderson, J. W. Long, R. M. Stroud, V. M. Cepak, V. M. Browning, D. R. Rolison, C. I. Merzbacher, *Nature* **2000**, *406*, 169.
[22] T. A. Schaedler, A. J. Jacobsen, A. Torrents, A. E. Sorensen, J. Lian, J. R. Greer, L. Valdevit, W. B. Carter, *Science* **2011**, *334*, 962.
[23] L. J. Gibson, M. F. Ashby, *Cellular Solids: Structure and Properties*, Cambridge Univ. Press, Cambridge **1997**.
[24] X. Lu, M. C. Arduini-Schuster, J. Kuhn, O. Nilsson, J. Fricke, R. W. Pekala, *Science* **1992**, *255*, 971.
[25] A. Cao, P. L. Dickrell, W. G. Sawyer, M. N. Ghasemi-Nejhad, P. M. Ajayan, *Science* **2005**, *310*, 1307.
[26] M. B. Bryning, D. E. Milkie, M. F. Islam, L. A. Hough, J. M. Kikkawa, A. G. Yodh, *Adv. Mater.* **2007**, *19*, 661.
[27] A. E. Aliev, J. Oh, M. E. Kozlov, A. A. Kuznetsov, S. L. Fang, A. F. Fonseca, R. Ovalle, M. D. Lima, M. H. Haque, Y. N. Gartstein, M. Zhang, A. A. Zakhidov, R. H. Baughman, *Science* **2009**, *323*, 1575.
[28] M. Xu, D. N. Fubata, T. Yamada, M. Yumura, K. Hata, *Science* **2010**, *330*, 1364.
[29] Z. P. Chen, W. C. Ren, L. B. Gao, B. L. Liu, S. F. Pei, H. M. Cheng, *Nat. Mater.* **2011**, *10*, 424.
[30] Y. Zhao, C. G. Hu, Y. Hu, H. H. Cheng, G. Q. Shi, L. T. Qu, *Angew. Chem., Int. Ed.* **2012**, *51*, 11174.
[31] H. Y. Sun, Z. Xu, C. Gao, *Adv. Mater.* **2013**, *25*, 2554.
[32] M. C. Lin, M. Gong, B. Lu, Y. P. Wu, D. Y. Wang, M. Y. Guan, M. Angell, C. X. Chen, J. Yang, B. J. Hwang, H. J. Dai, *Nature* **2015**, *520*, 325.
[33] F. M. Kong, J. D. LeMay, S. S. Hulsey, C. T. Alviso, R. W. Pekala, *J. Mater. Res.* **1993**, *8*, 3100.
[34] B. Wang, W. A. Abdulla, D. Wang, X. S. Zhao, *Energy Environ. Sci.* **2015**, *8*, 869.
[35] H. X. Ji, D. P. Sellan, M. T. Pettes, X. H. Kong, J. Y. Ji, L. Shi, R. S. Ruoff, *Energy Environ. Sci.* **2014**, *7*, 1185.
[36] M. Bastos-Neto, C. Patzschke, M. Lange, J. Möllmer, A. Möller, S. Fichtner, C. Schrage, D. Lässig, J. Lincke, R. Staudt, H. Krautscheid, R. Gläser, *Energy Environ. Sci.* **2012**, *5*, 8294.
[37] S. Cui, W. W. Cheng, X. D. Shen, M. H. Fan, A. T. Russell, Z. W. Wu, X. B. Yi, *Energy Environ. Sci.* **2011**, *4*, 2070.
[38] K. P. Loh, Q. L. Bao, G. Eda, M. Chhowalla, *Nat. Chem.* **2010**, *2*, 1015.
[39] F. Li, X. Jiang, J. J. Zhao, S. B. Zhang, *Nano Energy* **2015**, *16*, 488.
[40] H. P. Cong, J. F. Chen, S. H. Yu, *Chem. Soc. Rev.* **2014**, *43*, 7295.
[41] Z. Li, Z. Liu, H. Y. Sun, C. Gao, *Chem. Rev.* **2015**, *115*, 7046.
[42] B. Wicklein, A. Kocjan, G. Salazar-Alvarez, F. Carosio, G. Camino, M. Antonietti, L. Bergström, *Nat. Nanotechnol.* **2015**, *10*, 277.
[43] Y. S. Xie, S. Xu, Z. L. Xu, H. C. Wu, C. Deng, X. W. Wang, *Carbon* **2016**, *98*, 381.
[44] M. T. Pettes, H. X. Ji, R. S. Ruoff, L. Shi, *Nano Lett.* **2012**, *12*, 2959.
[45] S. Stankovich, D. A. Dikin, R. D. Piner, K. A. Kohlhaas, A. Kleinhammes, Y. Y. Jia, Y. Wu, S. T. Nguyen, R. S. Ruoff, *Carbon* **2007**, *45*, 1558.
[46] K. Mizuno, J. Ishii, H. Kishida, Y. Hayamizu, S. Yasuda, D. N. Futaba, M. Yumura, K. Hata, *Proc. Natl. Acad. Sci. USA* **2009**, *106*, 6044.